We are IntechOpen, the world's leading publisher of Open Access books Built by scientists, for scientists

6,900
Open access books available

186,000
International authors and editors

200M
Downloads

154
Countries delivered to

Our authors are among the

TOP 1%
most cited scientists

12.2%
Contributors from top 500 universities

CLARIVATE ANALYTICS

BOOK CITATION INDEX

INDEXED

WEB OF SCIENCE™

Selection of our books indexed in the Book Citation Index
in Web of Science™ Core Collection (BKCI)

Interested in publishing with us?
Contact book.department@intechopen.com

Numbers displayed above are based on latest data collected.
For more information visit www.intechopen.com

Radiation and Environmental Biophysics: From Single Cells to Small Animals

Yanping Xu

Additional information is available at the end of the chapter

Abstract

In this chapter, two of very unique and novel radiation technologies for modern radiobiology studies are reviewed. First of all, it is concentrated on the developments of accelerator-based particle microbeam system, which has been effectively used for studying the puzzle of "radiation-induced bystander effect." In addition, a recent published single-cell microbeam study, which is aiming to directly measure a cell's radio-sensitivity combining microbeam system with self-referencing biosensor, is included. Then, toward the study of realistic irradiation scenarios in radiation biology in particular, such as a nuclear attack for homeland security concerns or a potential large-scale radiological event, there would be a major need to ascertain, within a few days, the radiation doses received by tens or hundreds of thousands of individuals. Specifically, biological tests would need to be established to estimate the likelihood of such radiation exposure to result in serious health consequences; tests that would then be applied to decide on the correct treatments that might mitigate the short- and long-term health effects of such radiation exposure. However, because of the complexity and difficulty of conducting tests in such circumstance, innovative irradiation systems and technology are required. So the new developments of small animal irradiation system for evaluating the radiation risk and carrying out animal model radiobiology experiments within the mimicked radiation scenarios are covered in the second half of this chapter.

Keywords: Microbeam, Micro-biosensor, Single-cell irradiation, Small animal irradiation, Accelerator

1. Introduction

Historically, cancer and other health risks stemming from exposure to low-level radiation have been difficult to evaluate due to the high spontaneous frequency of age-related cancer and

degenerative diseases. With the dramatic increase in exposure of the human population to low-dose radiation either from diagnostic procedures, industrial applications, mining, cleanup of contaminated sites, and space travel, there has been a great scientific need for better estimates of the risks to such exposures. One of the driving forces behind the low-dose radiation research is developing specialized radiation technology and novel, versatile biophysics tools for such radiation biology and radiation physics studies.

2. Single-cell microbeam irradiation

2.1. Microbeam

For low-dose radiation circumstances which are extremely relevant to the environmental radiation exposure, individual cells hardly experience traversals by radiation particles. The biological effects of such low-dose radiation are unknown, and it is very difficult to study with conventional broad radiation beam exposure due to Poisson distribution of tracks. Also the cell-to-cell communication cannot be addressed directly because of the random radiation of broad beam particles. The microbeam system can overcome these difficulties. Microbeam is an irradiation system which delivers a certain number of particles with a micron-sized diameter spot to a chosen biological target, which allows damage to be precisely deposited within specific locations (e.g., nuclei or cytoplasm of single cells). Charged particle microbeams have been significant contributions to defining the biological targets of ionizing radiations. Also with microbeam, cell nuclear and cytoplasmic responses of targeted cells are established along with the responses of non-targeted bystander cells [1]. There is evidence that radiation-induced bystander signals between cells may originate with a diffusible mediator [2–4].

For more than 15 years, the Radiological Research Accelerator Facility (RARAF) of Columbia University has built and operated a charged particle microbeam facility capable of irradiating the nuclei of individual biological cells with as few as one helium ion or proton [5, 6]. The RARAF microbeam II is an updated system, and it is driven by a 5.5 MV HVEE Singleton Accelerator. The particles are ionized by a radio-frequency (RF) ion source inside the Singleton Accelerator and are accelerated from a DC high-voltage terminal to reach the desired energy. Then, the particle beam passes through a beam transport system to the beam end station where irradiation experiments take place. The beam transport system includes a few beam manipulation elements (**Figure 1**). The main beam slits and beam stop are used to eliminate unwanted ion beams, to limit the size of the beam entering a 90° bending magnet, and to stop the beam from entering the bending magnet when irradiations are not expected. The magnetic steering magnet is used to make fine adjustments, aiming the ion beam at the entrance of the bending magnet. The 90° bending magnet is used to bend the beam into the vertical direction. The beam deflector/shutter is an electrostatic system that steers the beam rapidly (~1 ms) to end the irradiation of a cell. The object aperture (~30 μm diameter) limits the initial beam size. A custom built electrostatic double-quadrupole triplet system [7] is used to focus the beam at the position of the cells to be irradiated. In front of the first triplet lens, an angular limiting aperture is used to eliminate particles entering at large angles to help reduce the diameter of the beam spot.

The beam exit window is a thin silicon nitride foil attached to a stainless steel disk, with thickness of either 500 nm or 100 nm (for a sub-micron beam spot) to minimize scattering the beam. The cell dish holder is designed to locate cells at the focusing plane of the microbeam and is in the view range of a customized microscope. An imaging/targeting system comprises a precision XYZ stage (MadCity Labs, Inc. WI), a Nikon Eclipse E600 microscope, and an attached PhotonMAX-512B EMCCD camera (Princeton Instruments, NJ). This equipment combination also allows us to image the wide range of fluorescent proteins that have been developed. A computer control program written in Visual Basic locates the cells, plated in a cell culture dish, and positions them for irradiation. While the RARAF microbeam is primarily used for charge particle irradiation, the accelerator can be used as source for neutral particle radiation, for example, neutron radiation [8–10].
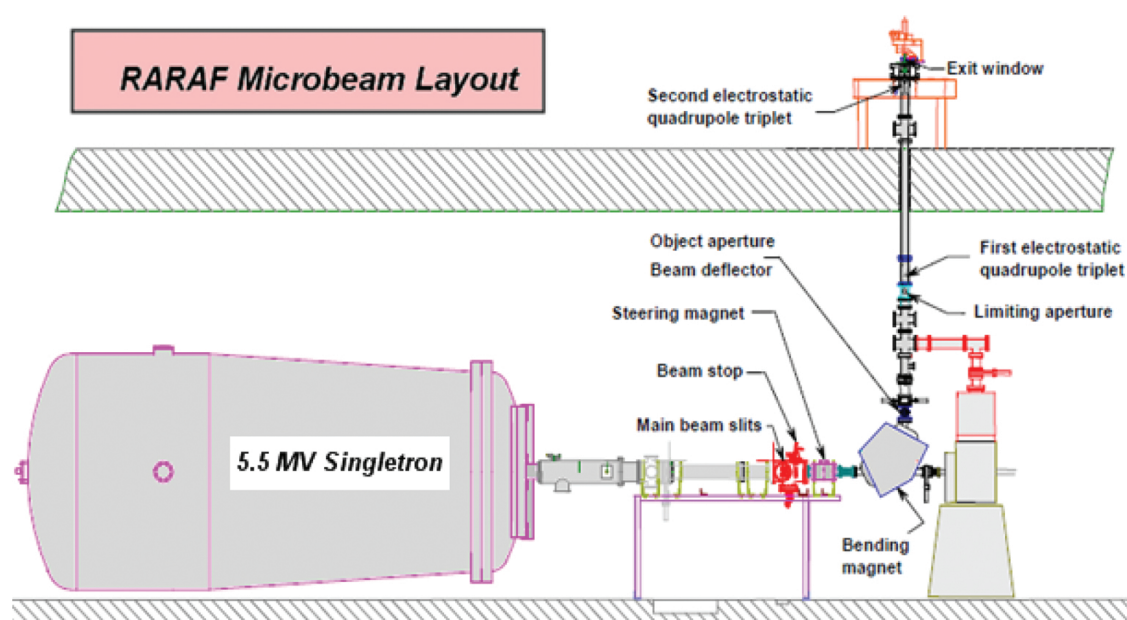

Figure 1. RARAF microbeam.

2.2. Single-cell microbeam irradiation with oxygen micro-biosensor

To physically demonstrate the radiation-induced oxygen flux changes outside the irradiated cell, a self-referencing amperometric electrochemical sensor was proposed for use with single-cell microbeam irradiation experiment. This type of micro-biosensor allows sensitive and non-invasive measurement of the flux of radical mediators, such as oxygen (or nitric oxide), in single cells. This is achieved by repeatedly moving the micro-biosensor/probe tip through the extracellular gradient at a known frequency and a known distance apart. This so-called self-referencing technique minimizes the measurement challenges caused by the random drift of the sensor output. In conjunction with a microbeam, it has the capacity to accurately detect selected ionic and molecular gradient changes surrounding a single cell with high spatial

resolution. The first radiobiology experiment was to analyze metabolic oxygen consumption in individual living lung cell after sub-cellular irradiation and to explore the radiation response of such cells. The self-referencing oxygen electrochemical system was developed at the Bio-Currents Shared Resource at the Marine Biological Laboratory (MBL), Woods Hole, MA. It was integrated with the RARAF single-particle, single-cell microbeam to form a single-cell irradiation response detection platform.

2.3. Oxygen self-referencing micro-biosensor

Self-referencing polarographic (SERP) micro-sensor technology was developed at the Bio-Currents Shared Resource [11–13]. These sensors are made of borosilicate glass capillaries (1B150, WPI) which are pulled to outer tip diameters of ~3 μm using a Sutter P-97 (Sutter Instrument, CA). Then, a 25-μm diameter gold wire (Alfa Aesar, Ward Hill, MA) is electro-chemically etched in an aqueous solution of 1N HCl to reduce the tip diameter to ~1 μm. After being rinsed with water and isopropyl alcohol, the etched Au wire is inserted into the capillary so that the wire protrudes slightly from the pipette tip. The electrode tip is dipped into UV curing epoxy (429, Dymax, Torrington, CT). The exposed Au electrode is then etched again (same conditions as above) to form a recessed electrode with a cavity 2–3 μm deep. Finally, the electrode is coated by dipping it in a solution of 10% cellulose acetate (30 kDa) for 60 s and drying for 5–10 min. The electrochemical sensor itself is attached to a BRC amperometric head stage via a modified BNC connecter. An L-shaped Ag/AgCl reference electrode, connected via a 3M KCl/5% agar bridge (reference probe) placed in the bulk solution, completes the circuit (**Figure 2**). Selectivity for amperometric electrodes is usually defined by the conditioning, operating voltage, and excluding membranes.
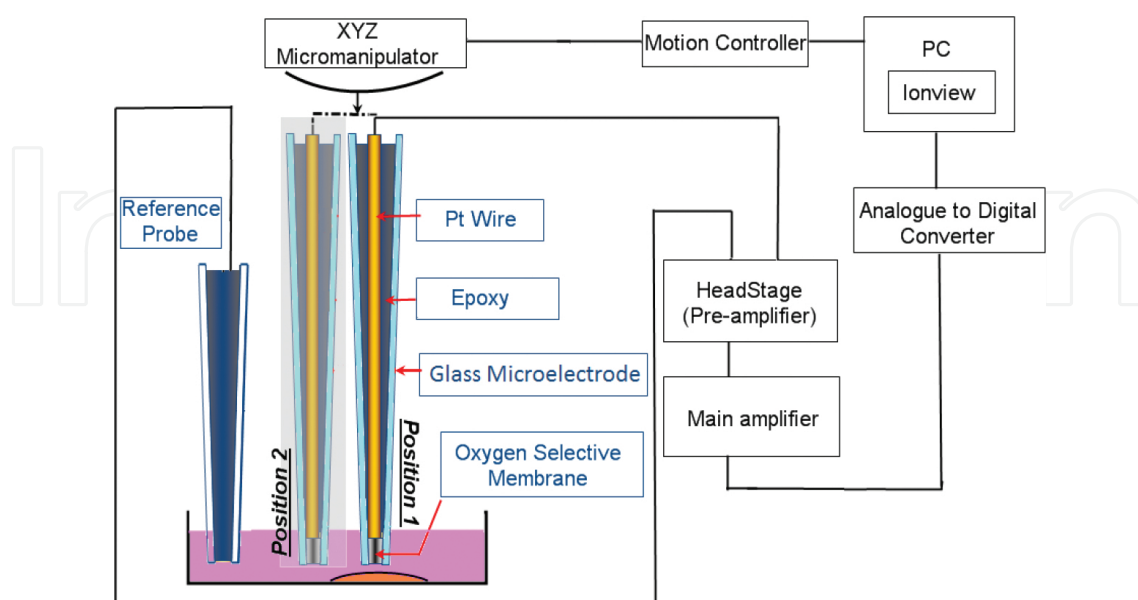

Figure 2. Self-referencing micro-biosensor detection system.

2.4. System integration

For single-cell irradiation response measurements, sensor access during and after irradiation for precision location of damage within single cells with the imaging system is crucial. Microprobe measurements without irradiation are usually performed on an inverted microscope giving open access from above for probe placement. With microbeam irradiation, there is a constraint from the exit window below the sample, so microscopy and probing must be done from above the sample. Access requires that the tip of the probe (microelectrode) approaches a single cell, at an angle of between 20° and 30°, to within microns of the plasma membrane. Access for the reference electrode is also required. Both the measuring probe and the reference electrode have body diameters of 1.5 mm, while the measuring tip is drawn to a point. A Nikon 10× long working distance (4 mm) dry microscope objective is placed with the probe in a sample dish. Because the probe approach angle is so severely constricted, the angle setting technique appropriate for an open-access system is completely inadequate. An offset hinge manipulator was designed (**Figure 3**) and built which allows rapid repeatable repositioning of the probe and simple angle adjustments. The hinge was constructed in a stacked configuration using high-precision flex pivots in such a way that angular settings between 10° and 60° can be set. In order to use the manipulator and the stacked hinge to satisfy our needs, a universal mounting car (Thorlabs, NJ) riding on an optical rail with an integrated robotic retraction mechanism is used. The probe manipulators are mounted accurately on the car for simple interchange. This robotic manipulator structure and the associated fully integrated control systems allow us to meet all the micromanipulation, and capillary probe placement needs in an efficient manner.

2.5. Measurement

2.5.1. Cell preparation

The human telomerase reverse transcriptase (hTERT) immortalized human small airway epithelial (SAE) cells were thawed from liquid nitrogen and cultured in fresh medium. Cells were diluted in fresh medium, and cultured cells were maintained at 37°C in a humidified 5%
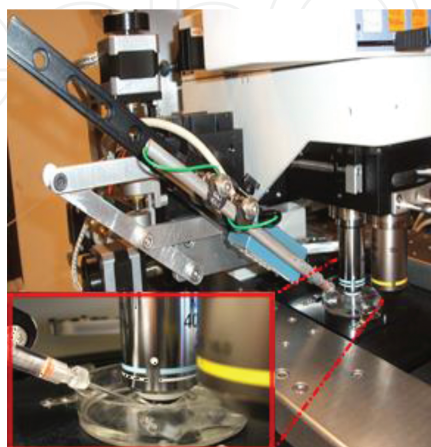

Figure 3. Electrochemical micro-sensor mounted on microbeam end station by the offset hinge system.

CO_2 incubator. The microbeam cell culture dishes were custom-made for cell growth and cell irradiation. They are made of Falcon 60 mm Petri dish, and a 0.25-inch diameter hole is drilled into the center of the dish bottom. The polypropylene film covered on the bottom of microbeam dish wells was treated with Cell-Tak (BD Biosciences) to enhance cell attachment. Also it allows the chosen radiation to get through to the cells while allowing them to be placed upright on the microbeam end stations with minimal distance between the dish bottom and beam exit window. Dishes were incubated at 37°C for 30 min and were then rinsed. Then, the cells were trypsinized and diluted to 1.5×10^4/ml (about 30 cells in a total volume of 2 μl medium). A sterile 18–22 mm square coverslip covered the well after cells in a droplet were plated using a micropipetter as close as possible to the center of the dish. The dishes were placed in an incubator until cells attached to the polypropylene. After cell attachment, the coverslips were removed and 5 ml more of medium was replenished to the dishes. Cells will typically flatten out within 1–3 h. The cells were stained by exposure to a 50 nM solution of the vital DNA-binding stain Hoechst 33342 for 30 min prior to radiation. This low stain concentration necessitates the use of an EMCCD camera (Princeton Instrument) to obtain a high-contrast image and allows rapid location of the cell nuclei to be hit, or not hit, as the experiment calls for during irradiation.

2.5.2. Radiation beam setup

Beam size and beam location were measured with a nickel knife edge scan [7]. Beam location was registered using scanning of fluorescent beads. This was done by placing a microbeam dish containing fluorescent beads on the stage. Then, an isolated bead was moved to the approximate beam position. A spiral energy loss mapping scan was conducted with a solid-state charge particle detector. Once the center of the beam was identified, the bead was moved to that position (the center of beam mapping) and the beam location was registered with the imaging system. The low-magnification pictures of the bead were taken, and a center-of-
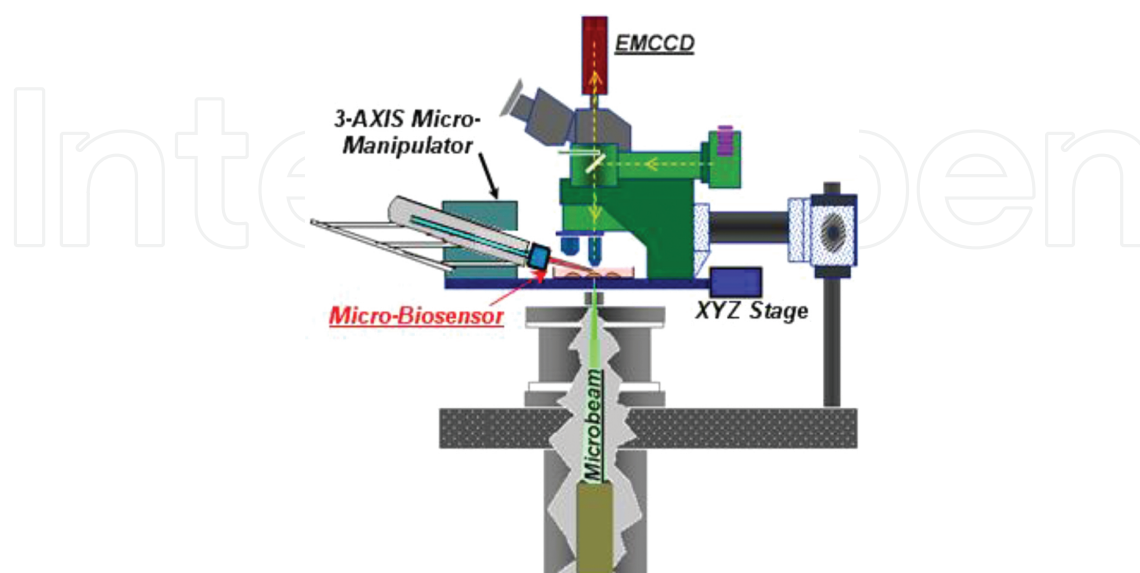

Figure 4. Measurement setup on microbeam end station.

gravity program routine was used to transfer the bead coordinates to the computer. Then, the cell dish was removed from incubator and was mounted on the microbeam stage. The chosen cell was moved to the registered beam position with an XYZ stage (MadCity Labs, Inc. WI), while monitored with a Nikon Eclipse E600 microscope and a reference picture was taken with an attached EMCCD camera (**Figure 4**). Then, the micro-electrochemical sensor and reference electrode were mounted on the XYZ stage, and the sensor/probe was carefully moved close to the cytoplasm (about 10–15 μm away) monitored with a Nikon 10× objective lens, and a background/control measurement was run for about 30 min with the sensor moved rapidly between two positions 15 μm apart at a frequency of 0.3 Hz. Data were collected at each pole position for approximately 1 s or 70% of the cycle time. The current signals were averaged at each position, and then, a differential current was obtained that can be converted into a directional measurement of flux using the Fick equation. Referencing the signals in this manner has the advantage that sources of interference caused by random drift and noise are effectively filtered from the signal and fluxes can be monitored in real time.

2.5.3. Radiation and real-time oxygen consumption measurement

During the single-cell microbeam irradiation, the current changes were monitored with biosensor in self-referencing mode. The number of helium ions was set at 20 or 30 in the microbeam irradiation protocol for this single-cell irradiation. The particle beam count rate was measured at about 200 per second. A pulser (Ortec Inc, TN) was used to simulate the real count rate and to control the beam shutter, because the 5.6 MeV helium ions cannot pass all the way through the cell and the medium (~1 mm thick) without being absorbed. In the cytoplasm irradiation experiments, an exclusion zone around each fluorescing nucleus is automatically generated to ensure that the cytoplasm target positions from one cell are not accidentally within the nucleus of an adjacent cell. Mutation induction caused by cytoplasmic irradiation has been reported using this technique. The image analysis system defines the long axis of each cell nucleus, after which the computer system delivers particles at two target positions along this axis, 6 μm away from each end of the cell nucleus. During the experiment, an in-house code with Matrox Genesis imaging library has been used to handle the images (subtract background, correct for illumination variation, locate cells, and record location of nearest frame).

2.6. Results

To detect physiologically driven molecular movements around the cell membrane, which is normally very small (fA current), the drift and background have to be taken care of with self-referencing technique. This requires extracting small electrical signals, fA differences (AC) on top of large offset signals 10s of pA (DC). With cells exposed to 10 μM anti-mycin, the basal cellular O2 flux was tested and the changes in oxygen concentration dependent current (DC changes) were detected. Then, both cytoplasm and nucleus irradiations with 100% cell radiation were conducted. **Figure 5** shows the background and drifting (DC) during the radiation. A very obvious O2 current change (AC) was recorded within seconds after cytoplasm irradiation. **Figure 6** shows the AC current change from two measurements with two
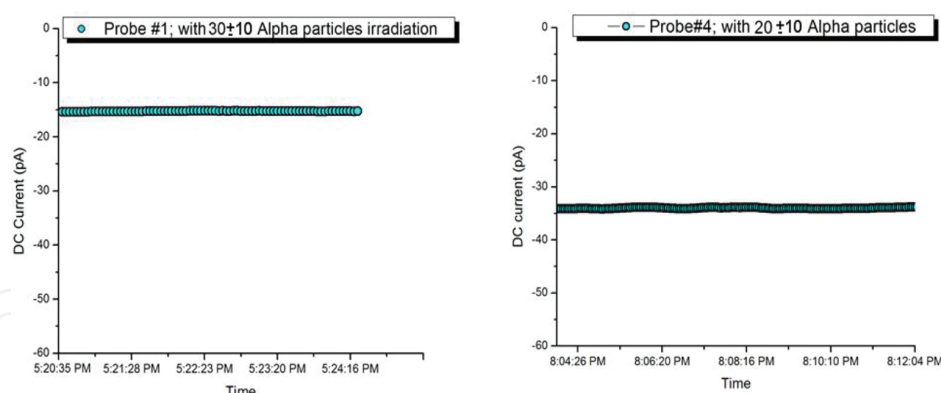
Figure 5. Self-referencing oxygen ion–selective probe result with alpha microbeam irradiation (DC).

different probes. The small changes in oxygen consumption could be extracted from the background oxygen concentration with the self-referencing method. A similar but relative small change was observed after nucleus irradiation. Without radiation, any of these large spikes cannot be seen on a long-time background measurement. Twelve measurements were conducted resulting in a success rate of ~30% as determined by the individual cell flux test because of the cell-to-cell variations and the uncertainty of the probe locations. The results indicate a role for mitochondrial damage following irradiation and enable further evaluations of the radiation-induced bystander effect. This effect is hypothetically due to the result of damage signals received by non-hit cells from hit cells. Establishing the mechanistic basis for such responses in the form of damage signaling from hit to non-hit cells and continued signaling has proven to be elusive. However, evidence for both oxygen- and nitrogen-based small molecules and mitochondrial dysfunction has been produced. The approach outlined in this study suggests biosensor mediators in the form of oxygen radicals, nitric oxide, and hydrogen peroxide can be directly measured at a single-cell level in both hit cells and bystander cells providing an incisive method of evaluating such evidence. This establishment of a non-invasive, self-referencing biosensor/probe system in conjunction with the RARAF microbeam provides an additional means for probing biological responsiveness at the level of individual cell, after precise sub-cellular targeting in hit cells and bystander cells.

3. An accelerator-based neutron small animal irradiation facility

3.1. Overview of IND-related radiation protection

Several scenarios of large-scale radiological events include the use of an improvised nuclear device (IND) that may produce a significant neutron component with the prompt radiation exposure [14]. Specifically, the prompt radiation from this type of detonation is expected to be qualitatively similar to that of the gun-type 15 kT device exploded over Hiroshima [15]. In order to assess the significance of the neutron exposure in dose reconstruction for this type of scenario and to allow characterization of novel neutron-specific biodosimetry assays, a new broad-energy neutron irradiator was designed [9] at the Columbia University RARAF.

This accelerator-driven neutron irradiator provides a broad-spectrum neutron field with energies from 0.2 to 9 MeV that mimics the evaluated energy spectrum produced in the detonation of the atomic bomb at Hiroshima at 1–1.5 km distance from ground zero [15]. At this distance, both survival and radiation exposure are expected to be sufficiently high to require triage for allocation of medical efforts; based on the Hiroshima data, the most survivors around this distance receive an appreciable neutron dose (up to 0.25 Gy [16]). However, the spectrum observed at this distance is significantly different from a standard reactor spectrum due to transport in the air, and has a larger component of low-energy neutrons. It is expected that this difference would have a significant impact on biodosimetric dose reconstruction.

The neutron field is produced by a mixed beam and composed of 5 MeV atomic and molecular ions of hydrogen and deuterium that is used to bombard a thick beryllium (Be) target. The latter is a well-known neutron-producing material not only because of its high neutron yield but also because of its stability and high specific heat. This mixed beam produces a neutron spectrum which is the sum of the spectra from the 9Be(d,n)10B and 9Be(p,n)9B reactions for all the incident ions (monatomic, diatomic and triatomic) and for energies from 5 MeV and down. In general, for monatomic 5 MeV projectiles, the 9Be(d,n)10B reaction provides a spectrum with higher-energy neutrons (above 1 MeV), while the 9Be(p,n)9B reaction primarily yields neutrons below 1 MeV. These nuclear reactions generate a combined neutron spectrum with a wide range of energies, which can then be used to irradiate biological samples and small animals (e.g., mice) for radiobiology studies. The beam composition in the present setup is approximately a 1:2 ratio of protons to deuterons. However, for other scenarios, the spectrum shape can be modified by adjusting the ratio of protons to deuterons and the incident beam energy.

As described elsewhere [17], the neutron spectra were evaluated by making combined measurements with a proton-recoil proportional counter [18] and liquid scintillator detector [19]. The measured recoil spectra were unfolded using maximum entropy deconvolution [20], based on Monte Carlo simulated detector response functions [21].

The dosimetry for the irradiations was performed using a custom tissue-equivalent (TE) gas ionization chamber, placed on the sample holder wheel. This chamber measures the total dose
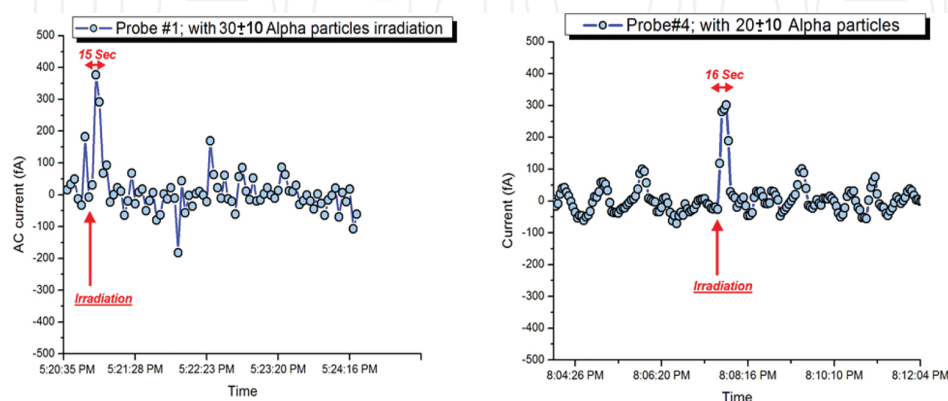

Figure 6. Self-referencing oxygen ion-selective probe result with alpha microbeam irradiation (AC).

in the mixed neutron and γ-ray field. To evaluate the ratio of neutron and γ doses, gamma-ray dosimetry was performed separately by replacing the ionization chamber with a compensated Geiger–Mueller dosimeter, which has a very low neutron response [22]. These measurements indicated that all neutron exposures, using this spectrum, are accompanied by a parasitic photon dose of about 21% of the total dose delivered.

In order to account for possible variations in the dose rate during irradiations, a second TE gas ionization chamber is placed in a fixed location on the beam axis, directly downstream of the neutron target and used as a monitor. All measurements are normalized to the signal from the monitor, which is used to determine the dose during irradiation.

In a realistic scenario, it is expected that the neutron dose will only be a small fraction of the total exposure (e.g., DS02 reported only 2% neutron dose at 1.5 km from the Hiroshima epicenter [16]). In order to mimic such a mixed field, a 250 kVp orthovoltage X-ray machine is located on site to allow irradiating samples with the necessary additional dose of photons.

To demonstrate the use of this facility, we present results from initial test using the in vitro cytokinesis-block micronucleus assay (CBMN, [23]) to measure the induction of micronuclei in peripheral human blood lymphocytes exposed to a range of neutron doses up to 1.5 Gy. The dose-response curves generated for micronuclei frequency indicated that the RBE of this neutron spectrum is between 3 and 5 compared to micronucleus yields induced by 250 kVp X-rays. As expected, these values fall between those for accelerator-generated energetic neutrons [24] and those for a reactor-based uranium fission spectrum [25].

3.2. Formation of a broad neutron spectrum

The key feature of our broad-energy neutron irradiator is its use of a mixed-gas ion source, with the spectrum depending on the ratio of gases in the mixture fed into the ion source. For this work, hydrogen and deuterium were combined at a ratio of 1:2 in one of the ion source gas supply cylinders and placed in the accelerator terminal. The ionization process of the mixed gas is complicated, as it generates many different ion combinations. To identify the actual ion beam ratios and to optimize the beam current, two different values of the gas valve control voltage were tested. The selected gas input parameter (percentage of maximum valve voltage) is used to control the pressure to provide sufficient beam current. To determine the ratio of the different ion species in our beam, we measured beam current at a 15° deflection, as a function of the field strength of the bending magnet. **Table 1** shows the fractions of the various atomic and molecular ions at two extremal pressures we can use (outside this pressure range, the beam current is too low or the ion source operation unstable). Several ion species (e.g., D^+ and H_2^+) cannot be separated magnetically because their magnetic rigidity is very close. As can be seen, increasing the valve voltage from 65.2 to 76.6% changed the ion ratios slightly for the molecular, but not atomic ions. As the major contributions to the spectrum come from the H^+ and D^+ ions, which vary by less than 2% over this range, we expect the spectrum will not vary significantly over this range of ion source parameters.

Gas valve control	65.2%	76.6%
Ion species		
D^+, H_2^+	35.75%	37.3%
D_2^+, H_2D	25.1%	16.7%
D_3^+	7.26%	12%
H^+	15%	16%
H_3^+	7.8%	2.2%
D_2H^+	8.9%	16%

Table 1. Ion species percentage for two different percentages of maximum gas control voltage.

Neutrons are generated as the particle beam impinges on a thick (500 μm) beryllium target. At this thickness, the 5 MeV deuterons and protons are completely stopped in the beryllium. The neutron energy spectrum obtained by this configuration was previously [9] modeled using MCNPX and more recently validated experimentally [17]. Briefly, an EJ-301 liquid-filled scintillation detector and a gas proportional counter filled with 3 atm of hydrogen were used for measuring neutron energies above and below 1.0 MeV, respectively. The combination of the two detection systems covers a wide-energy range, from 0.2 to >9 MeV. The recoil pulse height spectra acquired by the detector systems were carefully evaluated using different quasi-monoenergetic neutron beams (0.2–9 MeV) available at the RARAF accelerator, discriminating the γ-ray signals from the raw acquisition data with pulse rise time.

The two portions of the spectrum (obtained from the two detectors) were combined to form a kerma-weighted total spectrum (**Figure 7**). Overall, the obtained spectrum is similar to the one evaluated for Hiroshima [15], although it is slightly flatter. A more detailed discussion of the differences between our spectrum and Hiroshima appears elsewhere [17].
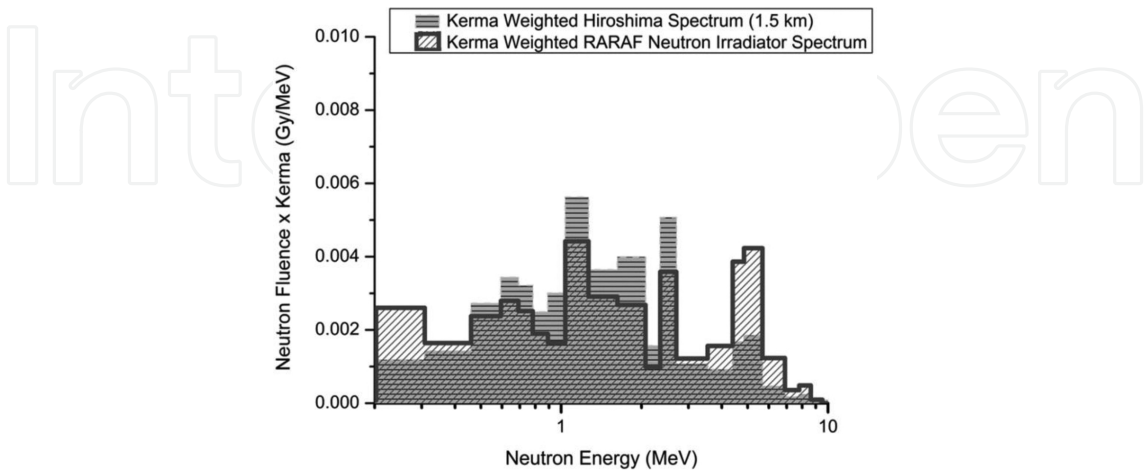

Figure 7. A comparison of the kerma-weighted neutron spectrum generated by us (hashed) with the one at 1.5 km from Hiroshima ground zero (gray).

3.3. Irradiation setup

Due to the requirement for a mixed H/D beam, the irradiation facility was set up using an un-deflected (0° angle) beam line in the RARAF accelerator facility (**Figure 8a**). The target assembly, shown in Figure 8b consists of a 2-mm-thick Cu disk onto which a 500-μm-thick beryllium foil was diffusion bonded. The dimensions of the copper disk were chosen so that it can be used in lieu of a standard 2.75″ CF gasket. The target is clamped between two Conflat flanges and doubles as a vacuum window. The target is cooled by water impinging on the copper backing plate [9].
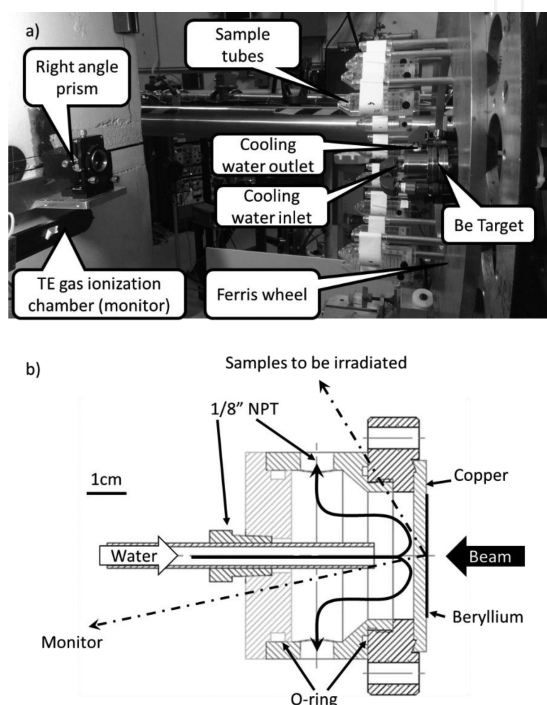

Figure 8. (a) Photo of the irradiation facility. Beam arrives from the right and impinges on the beryllium target generating neutrons. Samples to be irradiated (blood or mice) are placed in sample holders (shown here empty) and mounted on a Ferris wheel rotating around the target cooling chamber. At the left is the TE gas ionization chamber used as a beam monitor and the right angle prism used for aligning the beam line. (b) Cross-section of target and cooling chamber. Direction to the center of the sample holders (190 mm away) and the monitor chamber (610 mm away) are shown.

As the target cooling water lines, supporting structures, shielding, and other surrounding materials were seen to give about a 20% azimuthal variation in dose rate, a vertical Ferris wheel-like fixture (**Figure 8a**) is used to rotate the sample holder tubes (for either blood or mice) around the target. Customized tubes mounting from the rods on the wheel are used to hold the samples with a constant horizontal orientation at a distance of 190 mm from the target center. The fixture rotates up to 18 samples around the beam axis. The sample holders for both mice and ex-vivo irradiated blood are based on standard 50-ml conical centrifuge tubes (BD, Franklin Lakes, NJ) which were modified to allow hanging horizontally from rods on the wheel, so that the tubes maintain a constant orientation as the wheel rotates. This provides an isotropic irradiation, while maintaining the mice in an upright orientation, reducing stress.

During irradiations, the wheel is rotated at a speed of about 2 min per revolution and the dose rate adjusted so that the minimal dose is delivered in 10 rotations (20 min) with the sample tubes flipped end-to-end half-way through.

For pure photon exposure, a 250 kVp Westinghouse Coronado X-ray machine, placed within 15 m of the neutron irradiation facility, is used. This proximity allows for future mixed-field studies, where each sample may be immediately transported to the X-ray machine and irradiated after neutron exposure, with a time gap between the two irradiations of less than 5 min.

3.4. Neutron dosimetry

The total dose measurement for the IND-like neutron/gamma mixed-field irradiations was performed using a custom A-150 muscle TE gas ionization chamber (**Figure 9**), as described by Rossi et al. [26]. This chamber is intended for use in a mixed neutron and γ field measurement and features an interchangeable internal TE plastic sleeve. In the dosimetry measurements reported here, we used a 3.5-mm-thick sleeve to model the dose deposited at the center of the blood samples used. The chamber was filled with methane TE gas at ~700 mm Hg before the dosimetry measurement and sealed. The detector was then attached directly to an electrometer system and calibrated using a 50 mg 226Ra γ-ray source, which had been previously calibrated by the National Bureau of Standards. The dose rate was ~36 μGy/h at 1 m from the source. After calibration, the dosimeter was mounted on the sample wheel for the IND-like neutron irradiator at 60° with respect to the ion beam axis and 190 mm away from the target.
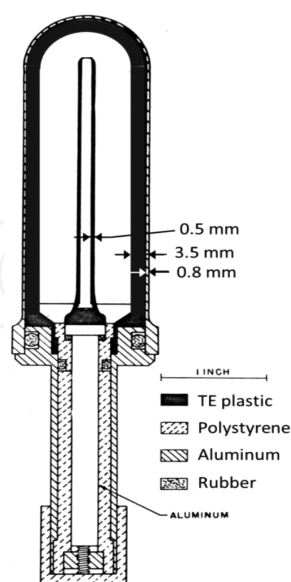

Figure 9. Custom TE gas ionization chamber for neutron dosimetry shown here with 3.5 mm TE plastic sleeve. This figure was originally published by Rossi et al. [26] and has been modified and re-published with the permission of *Radiation Research*.

To extract the dose due to neutrons, γ-ray dosimetry was performed separately with a compensated Geiger–Mueller dosimeter, which is 20 times more sensitive to photons than to monoenergetic neutrons in the range of 0.68–4.2 MeV [22]. The γ-ray dosimetry was conducted in the same manner as the total dose measurement and then subtracted from the latter. Since the γ-ray dose from the target rate is essentially isotropic, only inverse-square law corrections were performed.

The neutron dose rate at the sample position was $\sim 8.6 \times 10^{-2}$ Gy/h/μA, representing $\sim 79\%$ of the total dose rate, with the remaining 21% due to γ-rays. During the irradiation, the beam current was tuned to and kept at about 17.5 μA, which is equal to a neutron dose rate of ~ 1.5 Gy/h. Because of the possible variation of the dose rate relative to the beam current, a second TE gas ionization chamber was added as a monitor at a fixed location downstream of the neutron target at an angle of $\sim 12°$ relative to the ion beam direction. The monitor ionization chamber was filled with flowing TE gas, which was regulated with a constant-density control system. The incident primary particle beam current was recorded with an electrometer coupled to the end of the beam line, which is a Faraday cup-like isolated beam pipe with the target at the end.

3.5. Micronucleus assay analysis

Micronucleus formation in peripheral blood lymphocytes is a well-established marker of ionizing-radiation-induced DNA damage. We have used a recently established cytokinesis-block micronucleus (CBMN) assay protocol by Fenech [23] for accelerated sample processing by performing a miniaturized version of the assay in a multi-tube plate system [27].

Peripheral blood samples were collected from three healthy donors after informed consent (IRB protocol #AAAF2671) and exposed (3 ml aliquots) to nominal neutron doses of approximately 0.25, 0.5, 1, and 1.5 Gy (plus the concomitant 0.06, 0.1, 0.2, and 0.3 Gy of γ-rays). Blood sample aliquots were also exposed to 1, 2, and 4 Gy of 250 kVp X-rays.

Two hours post-irradiation, triplicate blood sample aliquots (50 μl) from each dose point were placed into culture in 1.0 ml 2D-barcoded matrix storage tubes (Thermo Scientific, Waltham, MA) with 500 μl of PB-MAX Karyotyping medium (Life Technologies, Grand Island, NY). Following 44 h of incubation, cytochalasin-B (Sigma Aldrich, St Louis, MO) was added at a final concentration of 6 μg/ml to inhibit cell cytokinesis and the tubes returned to the incubator. After a total incubation period of 72 h, the cells were harvested. Following hypotonic treatment, the cells were fixed using ice cold 4:1 fixative (methanol–acetic acid). The fixed samples were stored at 4°C (at least overnight), dropped on slides and stained with Vectashield mounting medium containing DAPI (Vector Laboratories, Burlingame, CA). The slides were imaged using a Zeiss fluorescent microscope (Axioplan 2; Carl Zeiss MicroImaging Inc., Thornwood, NY) with a motorized stage and a 10× air objective. Quantification of lymphocyte micronuclei yields were determined by automatic scanning and analysis by the MetaferMN Score software (MetaSystems, Althaussen, Germany). Between 1800 and 6000, binucleate cells were analyzed for each data point.

Figure 10a shows the comparison of the micronucleus yields for lymphocytes exposed to different neutron or X-ray doses. Overall, a dose-dependent increase in micronuclei yields was observed with increasing dose with both radiation fields with the yields induced by the X-rays following a linear quadratic behavior with dose and the neutron data following a linear trend.

The neutron data are actually induced by a mixed neutron + photon field. The dashed line shows that what we would expect from a pure neutron irradiation. This estimate was obtained by calculating excess micronucleus yields over controls from the photon component (21% of the total dose) based on the linear quadratic fit to the X-ray data. This value was then subtracted from the mixed-field yields at the same total dose. The resultant difference corresponds to the micronuclei yields that would be seen in a pure neutron irradiation.

3.6. Relative biological effectiveness (RBE) calculations

The potential biological effects and damage caused by radiation depend not only on the radiation dose received but also on the type of radiation. RBE was introduced to normalize the radiobiological effects caused by different types of radiation. RBE is defined as the ratio of photon dose (in our case 250 kVp X-rays) to the dose of the radiation field of interest (in our case neutrons), providing the same biological effect [28]. The biological effects caused by neutrons vary with energy and produce greater damage than X- or γ-rays. In general, for the same dose, neutrons are much more effective in damaging cells because neutron-induced secondary particles, for example, low-energy protons, have high LET (linear energy transfer) and photon-induced particles are electrons having low-LET. In this paper, we describe experiments aimed at measuring the neutron RBE for micronucleus formation in peripheral blood lymphocytes as part of the irradiator testing. Ongoing experiments using a variety of cytogenetic, transcriptomic, and metabolomic endpoints, in human blood and in mice, will be published separately.

The RBE for the mixed-field irradiation (neutrons and γ-rays; **Figure 10b**) was calculated from the linear and linear-quadratic regression curves, fitted to the neutron and X-ray data,
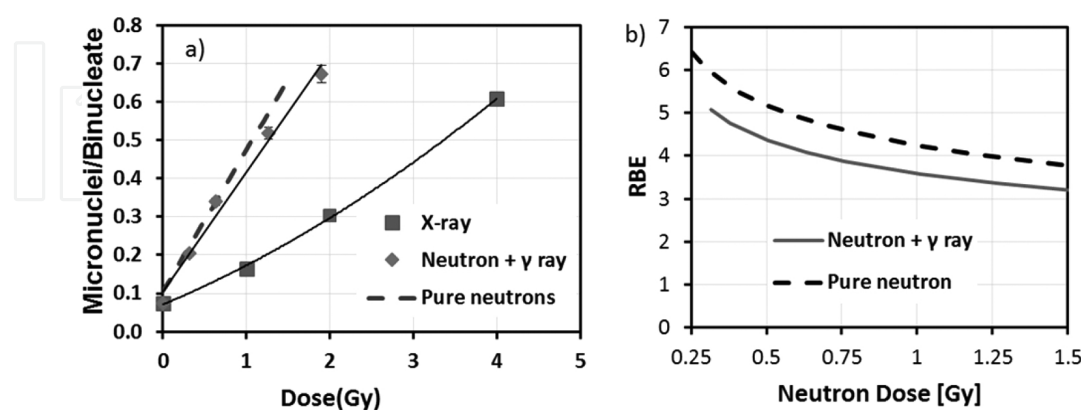
Figure 10. (a) Micronucleus frequency in human peripheral blood lymphocytes exposed *ex vivo* to neutrons or X-rays. The data show mean micronuclei per binucleate cell yields from three healthy volunteers. Error bars show ± SEM. The mixed-field yields plotted vs total dose (neutrons + γ-rays). The solid lines indicate a linear (neutrons) or linear-quadratic (X-rays) fit. The dashed line indicates the estimated pure neutron component. (b) RBE values for the mixed field and for the pure neutrons, calculated from panel a (see text for details).

respectively, by solving for the X-ray dose that would give the same micronucleus yield as a given dose of the mixed neutron/γ-ray field. The pure neutron RBE will be slightly higher than the RBE value of the mixed field. This was evaluated in the same way from the dashed line in **Figure 10a**.

The limiting RBE value of 4 is higher than the value of 2.5 reported for 6 MeV monoenergetic neutrons [24] but lower than the value of 6 calculated for a reactor fission spectrum [25], in accordance with what we would expect, based on the neutron energies.

4. Summary

A mixed beam of atomic and molecular deuterons and protons, accelerated to 5 MeV, impinges on a thick beryllium target, and the resultant neutron spectrum is the sum of the spectra from the 9Be(d,n)10B reaction (higher-energy neutrons) and the 9Be(p,n)9B reaction (lower-energy neutrons). The neutron energy spectrum is manipulated by adjusting the ratio of protons and deuterons to mimic the neutron spectra from an IND exposure for medical triage and bio-dosimetry studies. Specifically, it mimics the Hiroshima gun-type bomb spectrum at a relevant distance from the epicenter (1–1.5 km) and is significantly different from a standard reactor fission spectrum because the bomb spectrum changes as the neutrons are transported through air. The neutron spectrum of this irradiator was measured and is verified comparable with the Hiroshima bomb spectrum at 1.5 km. About 79% of the radiation dose is delivered by neutrons and He rest by γ-rays. A comparison of the biological effect of neutron and X-ray exposure on micronuclei yields in peripheral lymphocytes demonstrated that the IND-spectrum irradiator described above gives RBE values within the expected range.

Author details

Yanping Xu

Address all correspondence to: yx2132@cumc.columbia.edu

Radiological Research Accelerator Facility, Columbia University, Irvington, USA

References

[1] Hei TK, Ballas LK, Brenner DJ and Geard CR (2009) Advances in radiobiological studies using a microbeam. J Radiat Res, 50: A7–A12.

[2]   Shao C, Furusawa Y, Aoki M, Matsumoto H and Ando K (2002) Nitric oxide mediated bystander effect induced by heavy-ions in human salivary gland tumor cells. Int J Radiat Biol, 78(9): 837–44

[3]   Matsumoto H, Hayashi S, Hatashita M, Ohnishi K, Shioura H, Ohtsubo T, Kitai R,Ohnishi T and Kano E (2001) Induction of radioresistance by a nitric oxide-mediated bystander effect. Radiat Res, 155:387–396.

[4]   Azzam EI, de Toledo SM, Spitz DR and Little JB (2002) Oxidative metabolism modulates signal transduction and micronucleus formation in bystander cells from alpha-particle irradiated normal human fibroblast cultures. Cancer Res, 62(19):5436–42.

[5]   Gerard CR, Brenner DJ, Randers-Pehrson G and Marino SA (1991), Single-particle irradiation of mammalian cells at the radiological research accelerator facility: induction of chromosomal changes. Nucl Instrum Methods 11 B, 54, 411–416.

[6]   Randers-Pehrson G, Geard CR, Johnson GW and Brenner DJ (2001), The Columbia University single-ion microbeam. Radiat Res, 156, 13 210–214

[7]   Randers-Pehrson G, Johnson GW, Marino SA, Xu YP, Dymnikov AD and Brenner DJ (2009) The Columbia University sub-micron charged particle beam. Nucl Instrum Methods A, 609:294–299

[8]   Xu YP, Randers-Pehrson G, Marino SA, Bigelow AW, Akselrod MS, Sykora JG and Brenner DJ (2011) An accelerator-based neutron microbeam system for studies of radiation effects. Radiat Prot Dosim, 145:373–376

[9]   Xu Y, Garty G, Marino SA, Massey TN, Randers-Pehrson G, Johnson GW and Brenner DJ (2012) Novel neutron sources at the Radiological Research Accelerator Facility. J Instrum, 7, C03031, doi:10.1088/1748-0221/7/03/C03031.

[10] Bigelow AW, Randers-Pehrson G, Garty G, Geard CR, Xu Y, Harken AD, Johnson GW and Brenner DJ (2010) Ion, X-ray, UV and neutron microbeam systems for cell irradiation. AIP Conf Proc 1336: 351–355.

[11] Land SC, Porterfield DM, Sanger RH and Smith PJS (1999) The self-referencing oxygen-selective microelectrode: detection of transmembrane oxygen flux from single cells. J Exp Biol, 202: 211–218.

[12] Porterfield DM, Laskin JD, Jung SK, Malchow RP, Billack B, Smith PJS and Heck DE (2001) Proteins and lipids define the diffusional field of nitric oxide. Am J Physiol Lung C, 281: L904–L912.

[13] Kumar SM, Porterfield DM, Muller KJ, Smith PJS and Sahley CL (2001) Nerve injury induces a rapid efflux of nitric oxide (NO) detected with a novel NO microsensor. J Neurosci, 21: 215–220.

[14] Homeland Security Council, National Planning Scenarios (Final Version 21.3) (2006).

[15] Egbert SD, Kerr GD and Cullings HM (2007) DS02 fluence spectra for neutrons and gamma rays at Hiroshima and Nagasaki with fluence-to-kerma coefficients and transmission factors for sample measurements. Radiat Environ Biophys, 46: 311–25.

[16] Young RW, Egbert SD, Cullings HM, Kerr GD and Imanaka T (2005) Survivor dosimetry Part B. DS02 free-in-air neutron and gamma tissue kerma relative to DS86. Reassessment of the Atomic Bomb Radiation Dosimetry for Hiroshima and Nagasaki: Dosimetry System 2002.

[17] Xu Y, Randers-Pehrson G, Marino S, Garty G and Brenner D (2015) Broad energy range neutron spectroscopy with a liquid scintillator and a proportional counter: application to a neutron spectrum similar to that from an improvised nuclear device. . Nucl Instrum Methods A; 794, 234–239

[18] Tagziria H and Hansen W (2003) Neutron spectrometry in mixed fields: proportional counter spectrometers. Radiat Prot Dosim, 107, 73–93.

[19] Klein H (2003) Neutron spectrometry in mixed fields: NE213/BC501A liquid scintillation spectrometers. Radiat Prot Dosim, 107, 95–109.

[20] Reginatto M, Goldhagen P and Neumann S (2002) Spectrum unfolding, sensitivity analysis and propagation of uncertainties with the maximum entropy deconvolution code MAXED. Nucl Instrum Methods A, 476, 242–246.

[21] Pozzi SA, Flaska M, Enqvist A and Pázsit I (2007) Monte Carlo and analytical models of neutron detection with organic scintillation detectors. Nucl Instrum Methods A, 582, 629–637.

[22] Wagner EB and Hurst GS (1961) A Geiger–Mueller [gamma]-ray dosimeter with low neutron sensitivity. Health Phys, 5, 20–26.

[23] Fenech M (2007) Cytokinesis-block micronucleus cytome assay. Nat Protoc, 2, 1084–1104.

[24] Wuttke K, Müller W-U and Streffer C (1998) The sensitivity of the in vitro cytokinesis blocked micronucleus assay in lymphocytes for different and combined radiation qualities. Strahlentherapie und Onkologie (Radiotherapy and Oncology), 174, 262–268.

[25] Huber R, Schraube H, Nahrstedt U, Braselmann H and Bauchinger M (1994) Dose-response relationships of micronuclei in human lymphocytes induced by fission neutrons and by low LET radiations. Mutat Res Fundam Mol Mech Mutagen, 306, 135–141.

[26] Rossi HH, Bateman JL, Bond VP, Goodman LJ and Stickley EE (1960) The dependence of RBE on the energy of fast neutrons: 1. Physical design and measurement of absorbed dose. Radiat Res, 13, 503–520.

[27] Lue S, Repin M, Mahnke R and Brenner D (2015) Development of a high-throughput and miniaturized cytokinesis-block micronucleus assay for use as a biological dosim‐ etry population triage tool. Radiat Res. 184(2): 134–142.

[28] Hall EJ and Giaccia AJ, Radiobiology for the radiologist. 7th ed. Philadelphia: Lippin‐ cott Williams & Wilkins; 2012.